ISSN 0036-0244, Russian Journal of Physical Chemistry A, 2023, Vol. 97, No. 3, pp. 61–68. © Pleiades Publishing, Ltd., 2023.
Russian Text © The Author(s), 2023, published in Zhurnal Fizicheskoi Khimii, 2023, Vol. 97, No. 3, pp. 00000–00000.

CHEMICAL KINETICS AND CATALYSIS

Effect of Carbon on the Adsorption Properties of a $Co/MgAl_2O_4$ Catalyst for Carbon Monoxide Hydrogenation

G. V. Pankina[a],*, A. N. Kharlanov[a],, and P. A. Chernavskii[a]**

[a] *Faculty of Chemistry, Moscow State University, Moscow, 119992 Russia*

**e-mail: pankina5151@inbox.ru*

***e-mail: kharl@kge.msu.ru*

Received July 25, 2022; revised July 25, 2022; accepted August 8, 2022

Abstract—A study is performed of cobalt/$MgAl_2O_4$ catalysts promoted with glucose at Co/C molar ratios of 16.5, 3.2, and 1.6 via sequential deposition and codeposition. Magnetometry and IR spectroscopy of adsorbed CO show that raising the content of carbon in the catalyst contributes to the reduction of cobalt, regardless of how Co is introduced. Infrared spectroscopy reveals the main adsorption sites are cobalt cations and metallic Co. A strong contribution from adsorption sites characteristic of large Co particles is observed in systems synthesized via codeposition. Adsorption sites attributed to Co^{2+} and $Co^{\delta+}$ are structurally more homogeneous than ones attributed to metallic Co.

Keywords: glucose, supported Co catalysts, adsorption, promotion, magnesium–aluminum spinel, IR spectra, in situ magnetometry

DOI: 10.1134/S0036024423030214

INTRODUCTION

Along with iron-containing catalysts, cobalt catalysts supported on oxide supports (spinels in particular) are conventionally used in CO hydrogenation or Fischer–Tropsch synthesis (FTS). These catalysts are characterized by high activity, negligible rates of the water–gas shift reaction, and fairly strong resistance to deactivation [1, 2]. Cobalt-containing catalysts supported on highly porous inert supports are used in the selective production of C_2–C_4 alkenes, C_{5+} hydrocarbons, and liquid paraffins in CO hydrogenation (FTS), where metallic cobalt acts as an active site [1–3]. It is known that FTS catalysts must meet such basic requirements as the optimum size of cobalt particles, developed specific surface areas, and high reducibility [1, 4].

There are numerous ways of increasing the dispersion of cobalt. For example, a metal oxide (precursor) can be deposited on highly porous supports with large specific surface areas using highly soluble salts of cobalt nitrates to provide a high content of precursor in the catalyst [4, 5]. It is known that the codeposition of cobalt nitrates with chelating agents also reduces the size of metallic cobalt particles considerably [6–8]. In the $[Co(H_2O)_6(NO_3)_2]$ complex, the H_2O ligand is replaced with an organic ligand that forms a variety of chelating Co ions of the $[Co(ligand)(H_2O)_{6-x}]^{2+}$ form via a complexation reaction to increase the dispersion of Co [6]. Chinese scientists have studied the effect the coordination of a Co(II)–glycine complex has on the properties of Co/SiO_2 catalyst [7]. It was reported that glycine, which is an effective chelating agent, improves the dispersion of cobalt and activity in FTS at a glycine/Co^{2+} molar ratio of 3 in the Co(3gly)/SiO_2 complex, regardless of how the catalyst is synthesized. However, the Co(3gly)/SiO_2 complex synthesized via the reaction between glycine and cobalt hydroxide is characterized by homogeneous cobalt nanoparticles that are smaller and more stable than those synthesized according to a procedure in which glycine is mixed with a cobalt nitrate solution and silica gel is impregnated with the resulting solution [7, 8].

The effect precoating silica with carbon has on controlling the structure and characteristics of cobalt FTS catalysts was studied in [9]. It was found that coating SiO_2 with carbon stabilized fine cobalt oxide with the partial reduction to metallic cobalt upon heat treatment in an inert atmosphere. The size of cobalt oxide nanoparticles fell from 10–15 nm in conventional Co/SiO_2 catalyst synthesized without carbon precoating to 5–6 nm. Air calcination of samples synthesized with carbon precoating resulted only in a partial increase to 7–8 nm in the size of cobalt oxide nanoparticles and a uniform particle size distribution. Cobalt catalysts with high carbon contents exhibited strong catalytic characteristics. Encapsulating cobalt nanoparticles with carbon is considered to be the main

cause of the low activity of catalysts with a thin carbon layer. The subsequent removal of the carbon layer improved the catalysts' activity [10, 11].

The surface properties of a catalyst (its adsorption capacity in particular) have a strong effect on the reducibility of its active phase and thus on its catalytic activity in CO hydrogenation.

In this work, we explored the effect layer-by-layer promotion of a cobalt-containing catalyst supported on a magnesium–aluminum spinel with glucose as a carbon source has on its adsorption properties. Data from *in situ* magnetometry and IR spectroscopy of the effect adsorbed CO has on the adsorption and reduction of these carbon-promoted catalysts are compared.

EXPERIMENTAL

Catalyst Synthesis

The support of Co-containing catalysts promoted with glucose $C_6H_{12}O_6$ (referred to as GL in denoting the samples) was stoichiometric magnesium–aluminum spinel $MgAl_2O_4$ (SASOL Germany GmbH) of the Puralox MG 30 Spinel brand (referred to as S in denoting the samples) with $S_{sp} = 23$ m^2/g. We used a fraction with a particle size of <0.08 mm [12].

The supports were impregnated with a $Co(NO_3)_3{\cdot}5H_2O$ aqueous solution. The quantitative content of glucose in the impregnating solution was determined from the formation of x molecular layers of glucose ($x = 0$, 1, 5, and 10) in the catalyst's composition. Calculations were made with allowance for the spherical shape of a glucose particle with average size $d_{av} = 0.7$ nm and specific surface area $S_{sp} = 23$ m^2/g of the spinel. The surface area of 1 mol of glucose was determined and the amount of glucose required for the formation of a given number of monolayers on the catalyst surface was calculated.

Two sets of catalysts were synthesized that differed in how glucose $C_6H_{12}O_6$ was introduced into the catalyst (sequential deposition and codeposition).

The support for the first set of catalysts was prepared by preliminarily impregnating magnesium–aluminum spinel with an aqueous glucose solution of a given concentration. The mixture was dried for 4–5 h inside a rotary evaporator, and the dried samples were placed in a quartz reactor to ensure the decomposition of glucose to carbon. Calcination was done for 3 h at 450°C in a nitrogen atmosphere (gas flow rate of 10 mL/s) inside a muffle furnace using a temperature controller in the temperature-programmed mode (heating rate, 7 K/min). The supports prepared in this way were impregnated with a $Co(NO_3)_3{\cdot}6H_2O$ solution to ensure a Co content of 3 wt % and then dried and calcined under the above conditions. The catalysts of the first set were designated Co/(1)GLS, Co/(5)GLS, and Co/(10)GLS.

For the second set of catalysts, an $MgAl_2O_4$ support was initially impregnated with a mixture of $Co(NO_3)_3 \cdot 6H_2O$ and $C_6H_{12}O_6$ aqueous solutions of a given concentration and then dried in a rotary evaporator and calcined as described above. The catalysts of the second set were designated (Co1GL)/S, (Co5GL)/S, and (Co10GL)/S, respectively.

Calculations showed the cobalt-to-carbon Co/C molar ratio was 16.5 for the Co/(1)GLS and (Co1GL)/S samples, 3.2 for the Co/(5)GLS and (Co5GL)/S samples, and 1.6 for the Co/(10)GLS and (Co10GL)/S samples.

The samples were thoroughly ground to a powdery state in an agate mortar to select fractions with grain sizes of <0.08 mm.

Infrared Spectroscopy Studies

Diffuse reflectance infrared Fourier transform spectra were recorded on an EQUINOX 55/S FTIR spectrometer (Bruker). The powdered fraction of the test sample was placed in a quartz tube with a CaF_2 window and calcined at a temperature of 400°C (1 h in air and 2 h in a vacuum of at least 5×10^{-5} Torr). Gaseous CO was purified by passing it through a trap with liquid nitrogen and prolonged holding over a calcined zeolite. The difference spectra of adsorbed CO were obtained by subtracting the background spectrum from the experimental spectrum of a sample containing adsorbed CO with subsequent baseline correction using the OPUS 6.0 software (Bruker). Noise was subtracted digitally to improve the quality of the spectra.

In Situ Magnetometric Measurements

Magnetometry includes temperature-programmed reduction in hydrogen with simultaneous registration of magnetization (in situ) and magnetic granulometry (field dependences). Samples were studied on an original vibrating magnetometer (laboratory setup) in the in situ mode to measure the magnetization of ferromagnetic components formed during a chemical reaction [13]. Cobalt exhibits strong magnetic torque that determines the magnetization of samples. Magnetization (J) changes during processes with temporal variation in temperature, so we can observe the dynamics of reduction over time (dJ/dT), where the temperature depends linearly on time.

Catalysts weighing 10–20 mg were reduced in an H_2 stream while heating to a temperature of 600°C at a rate of 10 K/min in the measuring cell of a vibrating magnetometer. The cell was a quartz flow microreactor with a volume of 0.3 cm^3 that could be used to study topochemical transformations in situ [13]. A test sample was fixed rigidly between two porous quartz membranes, and the change in magnetization was recorded continuously while heating at a frequency of 1 Hz. Before each test, the magnetometer was cali-

brated against a special purity grade Co sample used as a standard. Upon reaching a given temperature, the catalyst was held in an isothermal mode until magnetization acquired a constant value testifying to the completion of reduction. After reduction, the samples were cooled in a stream of H_2 reducing gas at a rate of 10 K/min.

RESULTS AND DISCUSSION

In situ magnetometry was used to determine the sizes of metallic Co particles after reduction in H_2, the active site in CO hydrogenation, and the effect carbon had on the reducibility of cobalt. These data were used to calculate the particle sizes of the Co_3O_4 precursor. Magnetometry can be used to characterize the totality of processes that occur on the surface of a catalyst and in its bulk.

Granulometry was used to determine the magnetic characteristics of the systems. Magnetization J as a function of H (magnetic field magnitude) was measured for the reduced catalysts, and coercive force H_c and residual magnetization J_r were determined. Magnetic field magnitude H was varied in the range of ±8 kOe. Saturation magnetization was determined via extrapolation to a zero field. We calculated the concentration of Co in a reduced sample by assuming the saturation magnetization of bulk Co was 165 emu/g. Magnetic granulometry was conducted as described in [13]. The test sample was subjected to mild preliminary oxidation, and the coercive force was measured again. The coercive force exhibited an extreme dependence on the size of Co particles [14], with the maximum H_c value corresponding to $d = 20$ nm. The effective particle size of the metal fell upon oxidation, so two cases of change in H_c should be considered. A rise in H_c corresponds to the right branch of the $H_c(d)$ dependence, while a drop in H_c with a reduction in d corresponds to the left branch of the $H_c(d)$ dependence (Fig. 1).

When $d < 20$ nm, Co particles can be considered single-domain particles [14] for which $\gamma = 2J_r/J_s$, where J_r is residual magnetization, J_s is saturation magnetization, and γ is the fraction of nonsuperparamagnetic particles in the system [15]. We can obtain two $\gamma(T)$ values by measuring H_c at two temperatures:

$$\gamma_1 = 1 - \int_{V(T_1)}^{V_{20}} F(V;\mu,\sigma)dV \Big/ \int_{0}^{V_{20}} F(V;\mu,\sigma)dV,$$

$$\gamma_2 = 1 - \int_{V(T_2)}^{V_{20}} F(V;\mu,\sigma)dV \Big/ \int_{0}^{V_{20}} F(V;\mu,\sigma)dV,$$

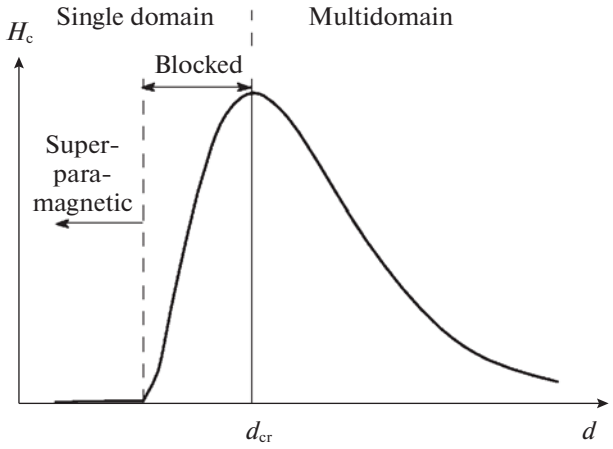

Fig. 1. Model dependence of coercive force on particle size (d, nm) [16].

and the particle size distribution can be found, assuming the particle size distribution is lognormal [16]:

$$F(V;\mu,\sigma) = \frac{1}{V\sigma(2\pi)^{1/2}}\exp\left[-\frac{(\ln V - \mu)^2}{2\sigma^2}\right],$$

The specific surface areas of Co and oxide Co_3O_4 were calculated using the formula

$$S_{sp} = 6M/\rho d,$$

where M is the corresponding weight (g/g of catalyst); ρ is the density of Co and Co_3O_4, respectively; and d is the average particle size of Co and Co_3O_4. We calculated the average particle sizes, specific surface areas, and specific volumes by assuming the Co and Co_3O_4 particles were spherical.

Table 1 lists the concentrations of metallic Co and average size of Co particles in test samples, determined from magnetic measurements, and the calculated specific surface areas and volumes of Co and Co_3O_4. We can see from these data that the tendency toward a reduction in the particle size of both cobalt oxide and metallic cobalt was maintained upon an increase in the concentration of carbon. At the same time, their specific surface area grew with sequential deposition, so it is logical to expect an increase in the adsorption capacity of the catalysts. In contrast, the specific surface area was reduced with codeposition.

The structural and electronic states of cations and atoms of cobalt on a sample's surface was determined via IR spectroscopy using adsorbed CO as the probe molecule. Unfortunately, the samples darkened considerably after reduction in hydrogen, hindering the use of IR spectroscopy, so we compared the state of a catalyst's surface before and after vacuum heat treatment. The surface and near-surface layer of a catalyst are partially reduced during vacuum heat treatment. We believe the laws governing the change in the state

Table 1. Content, average particle sizes (d, nm), and calculated specific surface areas (S, m^2/g) and specific volumes (V, cm^3/g) of Co and Co_3O_4

Catalyst	Co, wt %	d_{Co}	S_{Co}	$V_{Co} \times 10^3$	$V_{Co_3O_4} \times 10^3$	$d_{Co_3O_4}$	$S_{Co_3O_4}$
Co/S	2.3	8.4	1.8	2.6	5.1	10.5	2.9
Co/(1)GLS	1.6	15	0.7	1.8	3.6	19	1.1
Co/(5)GLS	1.2	7.6	1.1	1.3	2.7	9.5	1.7
Co/(10)GLS	3	>20	—	3.4	6.7	>25	—
(Co1GL)/S	2	7.4	1.8	2.2	4.4	9	2.9
(Co5GL)/S	0.6	6.3	0.64	0.7	1.3	8	1
(Co10GL)/S	0.4	>20	—	0.4	0.9	>25	—

of cobalt during deep reduction in a hydrogen atmosphere and the partial reduction of the near-surface layer under conditions of a vacuum heat treatment are similar, and vacuum heat treatment is the initial stage of reduction of cobalt in the bulk.

Figure 2 shows the difference IR spectra of CO adsorbed at room temperature and CO pressures of 5, 20, and 50 Torr on a Co/S catalyst and catalysts synthesized via the sequential deposition of carbon and cobalt on spinels. We can see from Fig. 2a that the spectra of carbon monoxide adsorbed on the surface of a Co/S sample at room temperature were formed by the superposition of several absorption bands. The group of overlapping absorption bands at 2135, 2152–2153, and 2166 cm^{-1} can be attributed to carbonyl complexes on Co^{2+} cations in different coordination environments [17], while the absorption bands at 2180–2181 cm^{-1} were attributed to complexes with Co^{3+} cations [18–21]. According to [18], the absorption band at 2152 cm^{-1} also corresponds to CO complexes with Co^{2+} cations, the coordination spheres of which include oxygen vacancies. The intense asymmetric absorption band at 2070 cm^{-1} can be attributed to CO complexes with $Co^{\delta+}$ cations ($\delta < 1$) [18–21]. The asymmetry of this absorption band suggests it corresponds to an unresolved superpositioning with absorption bands at lower frequencies. Absorption in the region of 1983–1995 cm^{-1} was attributed to carbonyl complexes with Co^0 atoms [17].

The spectrum of CO adsorbed on the Co/(1)GLS sample (Fig. 3b) was also formed by a superpositioning of three groups of absorption bands. Note that the contribution from absorption bands corresponding to complexes with Co^{2+} (2165–2168, 2151–2155, 2134–2137 cm^{-1}) was considerably larger. In terms of intensity, it exceeds the superpositioning of the absorption bands at 2070 and 2058 cm^{-1} attributed to complexes of CO with $Co^{\delta+}$. Absorption bands at 1980–1982, 2002–2008, and 2032–2037 cm^{-1} are observed in the low-frequency region of the spectrum. As noted above, the absorption band at 1980 cm^{-1} can be attributed to CO complexes with Co^0 atoms. It is assumed [21] this frequency corresponds to complexes with cobalt atoms on the surfaces of large particles, while the absorption band of higher frequency at 2002–2008 cm^{-1} can be attributed to CO adsorption on isolated cobalt atoms. The data in Table 1 show the size of particles of metallic cobalt in the samples reduced in hydrogen was 8.4 and 15 nm for Co/S and Co/(1)GLS, respectively.

The nature of the absorption bands at 2032–2037 cm^{-1} can be debated. We believe the emergence of this absorption band is associated with carbon in the composition of the catalyst and could correspond to CO adsorption on $Co^{\delta+}$ in the composition of cobalt carbide.

The contribution from high-frequency bands in the region of 2100–2170 cm^{-1} was reduced considerably when the concentration of carbon was raised to a content corresponding to Co/C = 3.2 (Co/(5)GLS sample, Fig. 2c), and the bands at 2168–2172 and 2134–2137 cm^{-1} disappeared from the spectrum. The observed superpositioning came mostly from absorption bands at 2141 and 2154–2156 cm^{-1} with a small contribution from the absorption band at 2112 cm^{-1}. The superpositioning of the absorption bands at 2044–2047 and 2071 cm^{-1} corresponding to CO complexes with $Co^{\delta+}$ cations came to dominate in the spectrum. In the low-frequency part of the spectrum, this intense complex absorption band was superimposed on absorption bands at frequencies of 2014–2016 cm^{-1} corresponding to CO complexes with isolated Co atoms, absorption bands at 1982–1987 cm^{-1}, and new absorption bands at 1933–1945, 1920, 1872, and 1826 cm^{-1}. Similar bands were observed by the authors of [17, 22, 23] upon prelonged holding of Co_3O_4 in a CO atmosphere. They correspond to CO complexes with cobalt atoms localized on metallic cobalt particles or clusters with metal structure.

Upon reduction in hydrogen, the size of Co particles in this sample fell to 7.6 nm, relative to that of the Co/(1)GLS sample (15 nm) (Table 1).

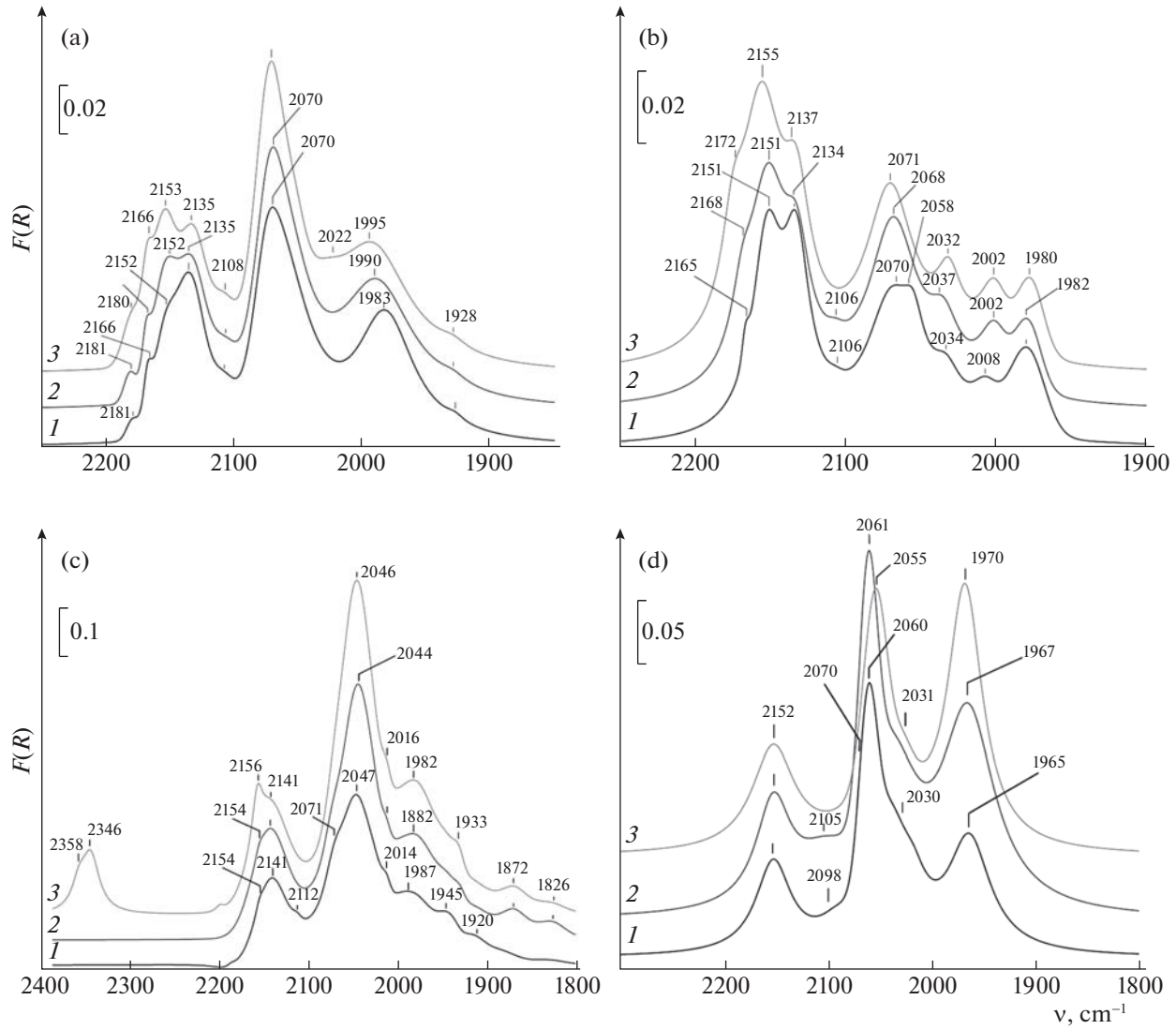

Fig. 2. Difference IR spectra of CO adsorbed at room temperature on (a) the Co/MA, (b) Co/(1)GLS, (c) Co/(5)GLS, and (d) Co/(10)GLS catalysts; CO pressure: (*1*) 5, (*2*) 20, and (*3*) 50 Torr.

The optical characteristics of the sample deteriorated substantially when the concentration of carbon was raised to Co/C = 1.6 (Co/(10)GLS sample, Fig. 2d). Tests showed the surface of the sample was apparently carbonized, so information about the low-intensity components of the spectrum was lost after filtering out noise. We can see the ratio of the contributions from CO complexes with Co^{2+} (the absorption band at 2152 cm^{-1}) and $Co^{\delta+}$ (the absorption band at 2055–2061 cm^{-1}) is comparable to the one for the Co/(5)GLS sample. However, the contribution from complexes with Co^0 atoms on the surfaces of metallic cobalt particles grew considerably (the absorption band at 1965–1970 cm^{-1}). There was also a contribution from the absorption band at 2030 cm^{-1} of CO complexes with isolated cobalt atoms. Magnetometry (Table 1) revealed the size of Co particles grew to >20 nm after reduction in hydrogen.

Compared to the Co/S sample, introducing carbon into a catalyst in a concentration equivalent to one precursor monolayer (Co/C = 16.5) via codeposition with cobalt (Fig. 3a, sample (Co1GL)/S) also raised the contribution from CO complexes with Co^{2+} relative to those of complexes with $Co^{\delta+}$. In contrast to the Co/(1)GLS sample, however, no contribution is observed from the absorption bands at 2165 and 2172 cm^{-1}. The maximum of the absorption bands of CO complexes with $Co^{\delta+}$ is observed for the absorption band at 2050–2053 cm^{-1}, below the maximum for the analogous absorption bands of the Co/(1)GLS sample synthesized via sequential deposition. Note too that superpositioning of the absorption bands at

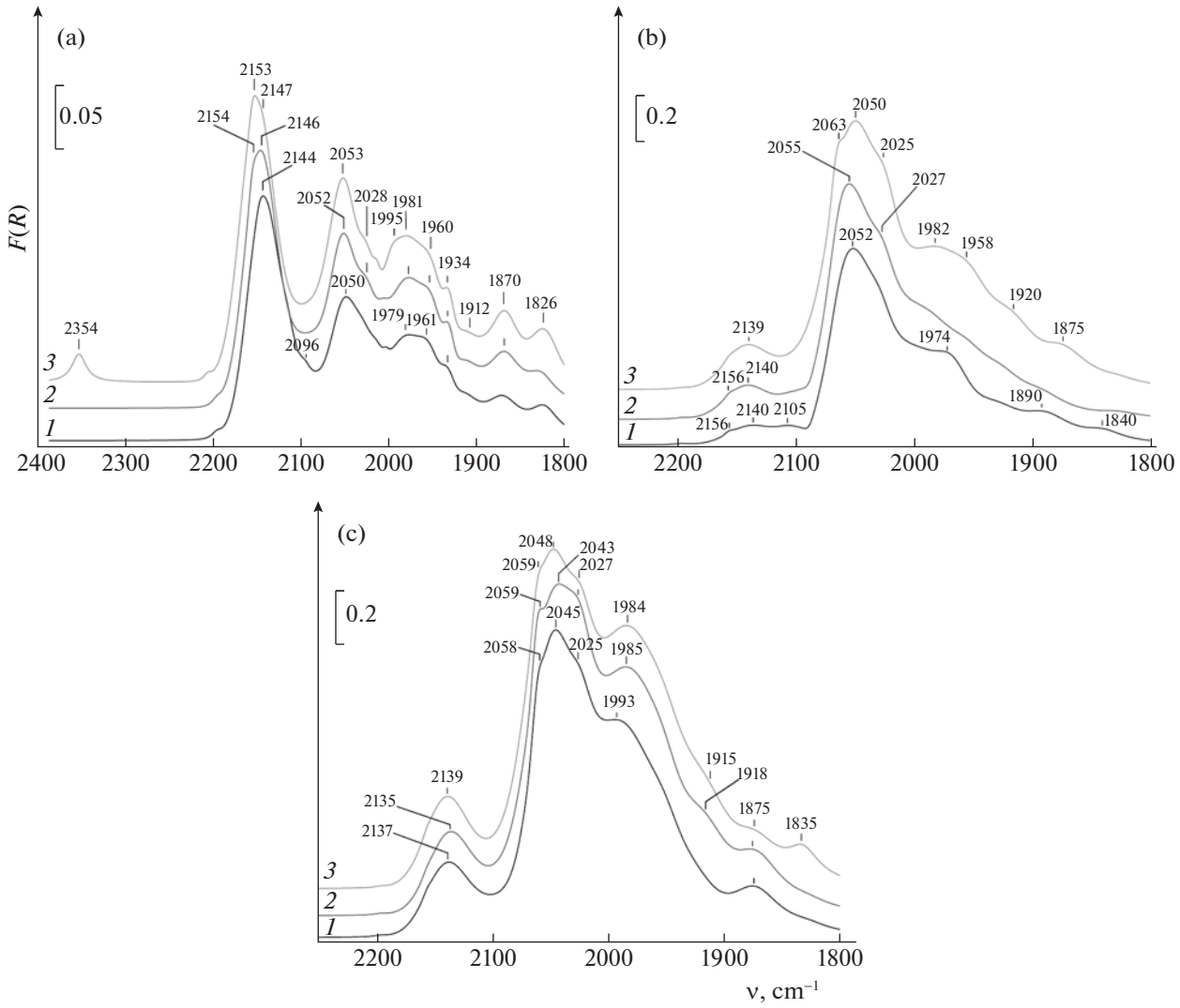

Fig. 3. Difference IR spectra of CO adsorbed at room temperature on (a) the (Co1GL)/S, (b) (Co5GL)/S, and (c) (Co10GL)/S catalysts. CO pressure: (*1*) 5, (*2*) 20, and (*3*) 50 Torr.

2058 and 2070 cm^{-1} is observed for the Co/(1)GLS sample with the absorption band at 2070 cm^{-1} predominating at high CO pressures, while the absorption band at 2070 cm^{-1} is missing from this spectrum. The spectrum thus does not contain high-frequency components of CO complexes with either Co^{2+} or $Co^{\delta+}$. In the low-frequency part of the spectrum, the number of bands is higher than for an analogous sample synthesized via sequential deposition. The superpositioning of absorption bands at 1995, 1979–1981, and 1960–1961 cm^{-1} is observed. The band at 1995 cm^{-1} can be attributed to CO complexes with isolated Co atoms; all other bands listed above are attributed to interaction between atoms on metal particles and clusters with the structure of metal particles. Like the spectrum of CO adsorbed on the Co/(5)GLS sample synthesized via sequential deposition, the contribution from absorption bands at 1934, 1912, 1870, and 1826 cm^{-1} is substantial; i.e., the adsorption sites attributed to Co^{2+} and $Co^{\delta+}$ are structurally more homogeneous than those attributed to Co^0 atoms.

In the spectrum of CO adsorbed on (Co5GL)/S (Fig. 3b), the contribution from the absorption bands of complexes with Co^{2+} cations (the superpositioning of bands at 2156, 2139–2140, and 2105 cm^{-1}) is much lower than those for the (Co1GL)/S sample and the analogous Co/(1)GLS synthesized via the sequential introduction of glucose and cobalt. The absorption bands at 2050–2055 and 2063 cm^{-1} of CO complexes with $Co^{\delta+}$ predominate in the spectrum. The contribution from CO complexes with Co^0 is also substantial.

When the concentration of carbon was raised to Co/C = 1.6 (sample (Co10GL)/S), the spectrum of

adsorbed CO (Fig. 3c) was comparable to the spectrum of CO adsorbed on the (Co5GL)/S sample, but the contribution from the absorption bands at 1984 cm^{-1} and lower frequencies grew in the region below 2000 cm^{-1}.

CONCLUSIONS

Data obtained in two ways were compared. It was shown that introducing carbon into the catalyst's composition in an amount equivalent to one precursor monolayer (Co/C = 16.5) results in a much larger contribution to the spectrum from complexes with Co^{2+} cations, relative to those from complexes with $Co^{\delta+}$ cations. How the carbon is introduced does not matter. The reduction of cobalt is therefore negligible with this small amount of carbon. The absorption bands at 2002–2008 cm^{-1} in the spectrum of the Co/(1)GLS sample also indicates a considerable number of isolated cobalt atoms, while the spectrum of the (Co1GL)/S sample synthesized via codeposition exhibits mostly the absorption bands characteristic of complexes with cobalt atoms contained in clusters with a metal structure.

Regardless of the means of synthesis, raising the concentration of carbon to a content equivalent to five precursor monolayers (Co/C = 3.2) substantially reduced the contribution from complexes with Co^{2+} cations and increased those from complexes with Co^{+} cations and metallic cobalt. Cobalt was thus reduced more readily in these systems than in ones containing no carbon and those that contained carbon in the concentration of one precursor monolayer.

Note that the contribution from complexes with Co^0 in the composition of clusters and the metal phase for the (Co5GL)/S sample was larger than the one for the Co/(5)GLS system. It is possible that cobalt had stronger reducibility in the system synthesized via co-introduction with carbon.

The contribution from complexes with metallic cobalt grew at a concentration of carbon equivalent to ten precursor monolayers (Co/C = 1.6), indicating even stronger reducibility of cobalt. However, the contribution from absorption bands in the region of 2010–2030 cm^{-1}, which corresponds to CO complexes with isolated cobalt atoms, fell in the Co/10GLS system. It is likely that cobalt segregated into large particles in this system.

The relatively low intensity of the absorption bands of CO complexes with Co^{3+} cations can be attributed to the reduction of Co_3O_4 to CoO in near-surface layers forming CO_2 under the conditions of vacuum heat treatment [23–25].

According to data obtained by both *in situ* magnetometry and IR spectroscopy of adsorbed CO, an increase in the carbon content contributed to the reduction of cobalt, regardless of how the Co was introduced. However, the data in Table 1 suggest the reduction of the catalysts synthesized via sequential promotion with carbon was more efficient due to adsorption.

The main sites of CO adsorption were cobalt cations and metallic Co. A substantial contribution from adsorption sites characteristic of large particles of metallic Co was observed in systems synthesized via codeposition. The adsorption sites attributed to Co^{2+} and $Co^{\delta+}$ were typically more homogeneous, while those attributed to Co^0 were heterogeneous. Our magnetometry data largely confirmed the results from IR spectroscopy. However, it should be remembered that the data obtained via IR spectroscopy correspond to the initial stage of reduction under mild conditions of vacuum heat treatment and represent processes that occur exclusively on the surfaces and in the near-surface layers of the catalysts, while magnetometry data can represent processes that occur in the bulk of the system as well.

CONFLICT OF INTEREST

The authors declare they have no conflicts of interest.

REFERENCES

1. A. Y. Khodakov, W. Chu, and P. Fongarland, Chem. Rev. **107**, 1692 (2007).
2. Z. Y. Qi, L. N. Chen, S. C. Zhang, et al., Appl. Catal. A: Gen. **602**, 117701 (2020).
3. Q. Zhang, J. Kang, and Y. Wang, ChemCatChem **2**, 1030 (2010).
4. J. S. Girardon, G. Quinet, A. Griboval-Cocstant, et al., J. Catal. **248**, 143 (2007).
5. L. Shi, C. Y. Zeng, Q. H. Lin, et al., Catal. Today **228**, 206 (2014).
6. A. Jos van Dillen, R. J. A. M. Terörde, D. J. Lensveld, et al., J. Catal. **216**, 257 (2003).
7. Qing-Qing Hao, Min Hu, Zhi-Xia Xie, et al., Catalysts **10**, 1295 (2020).
8. T. Machizuki, T. Hara, N. Koizumi, and M. Yamada, Appl. Catal. A: Gen. **317**, 97 (2007).
9. K. Cheng, V. Subramanian, A. Carvalho, et al., J. Catal. **337**, 260 (2016).
10. P. Munnik, P. E. de Jough, and K. P. de Jong, J. Am. Chem. Soc. **136**, 7333 (2014).
11. J. P. Breejen, J. R. A. Sietsma, H. Friedrich, et al., J. Catal. **270**, 146 (2010).
12. G. V. Pankina, A. N. Kharlanov, and P. A. Chernavskii, Russ. J. Phys. Chem. A **96**, 969 (2022).
13. P. A. Chernavskii, G. V. Pankina, and V. V. Lunin, Russ. Chem. Rev. **80**, 579 (2011).
14. J. Sort, S. Surinach, and J. S. Munoz, Phys. Rev. B **68**, 014421 (1997).
15. A. Barbier, A. Tuel, I. Arcon, et al., J. Catal. **200**, 106 (2001).

16. P. A. Chernavskii, Chu Vei, A. Yu. Khodakov, et al., Russ. J. Phys. Chem. A **82**, 951 (2008).
17. A. Davydov, *Molecular Spectroscopy of Oxide Catalyst Surfaces* (Wiley, New York, 2003).
18. J. Jansson, A. E. C. Palmqvist, E. Fridell, et al., J. Catal. **211**, 387 (2002).
19. S. Todorova, V. Zhelyazkov, and G. Kadinov, React. Kinet. Catal. Lett. **57**, 105 (1996).
20. Y. J. Mergler, A. van Aalst, J. van Delft, and B. E. Nieuwenhuys, J. Catal. **161**, 310 (1996).
21. G. Busca, R. Guidetti, and V. Lorenzelli, J. Chem. Soc., Faraday Trans. **86**, 989 (1990).
22. T. T. Chiong and A. A. Davydov, Zh. Fiz. Khim. **63**, 271 (1989).
23. Y. J. Mergler, A. van Aalst, J. van Delft, and B. E. Nieuwenhuys, J. Catal. **161**, 310 (1996).
24. G. Busca, R. Guidetti, and V. Lorenzelli, J. Chem. Soc., Faraday Trans. **86**, 989 (1990).
25. M. Schonnenbeck, D. Cappus, J. Klinkmann, et al., Surf. Sci. **347**, 337 (1996).

Translated by M. Timoshinina

SPELL: OK